Biophysical Journal Volume 96 March 2009 2029–2042

A Thermodynamic Model of the Cardiac Sarcoplasmic/Endoplasmic Ca^{2+} (SERCA) Pump

Kenneth Tran,[†*] Nicolas P. Smith,[‡] Denis S. Loiselle,[†§] and Edmund J. Crampin[†¶]
[†]Auckland Bioengineering Institute, [§]Department of Physiology, [¶]Department of Engineering Science, University of Auckland, New Zealand; and [‡]University Computing Laboratory, Oxford University, United Kingdom

ABSTRACT We present a biophysically based kinetic model of the cardiac SERCA pump that consolidates a range of experimental data into a consistent and thermodynamically constrained framework. The SERCA model consists of a number of sub-states with partial reactions that are sensitive to Ca^{2+} and pH, and to the metabolites MgATP, MgADP, and Pi. Optimization of model parameters to fit experimental data favors a fully cooperative Ca^{2+}-binding mechanism and predicts a Ca^{2+}/H^{+} counter-transport stoichiometry of 2. Moreover, the order of binding of the partial reactions, particularly the binding of MgATP, proves to be a strong determinant of the ability of the model to fit the data. A thermodynamic investigation of the model indicates that the binding of MgATP has a large inhibitory effect on the maximal reverse rate of the pump. The model is suitable for integrating into whole-cell models of cardiac electrophysiology and Ca^{2+} dynamics to simulate the effects on the cell of compromised metabolism arising in ischemia and hypoxia.

INTRODUCTION

Quantitative computational modeling has proven to be an important and successful tool for the analysis of electrophysiology and Ca^{2+} handling dynamics in cardiac myocytes during normal metabolic function (1). Recent examples of electrophysiological modeling frameworks formulated for a range of animal species include the models of Nobel et al. (2), Winslow et al. (3), Faber and Rudy (4), Matsuoka et al. (5), and ten Tusscher and Panfilov (6). These frameworks include descriptions of two key energy-dependent transporters: the Na^{+}/K^{+} and the SERCA pumps, which play important roles in cell electrophysiology and Ca^{2+} dynamics, respectively. These models, however, become limited when attempting to simulate conditions brought about by changes in the energetic state of the myocyte such as ischemia, where cell metabolism is compromised. To overcome this issue of metabolic insensitivity, we have developed a new quantitative model of the cardiac SERCA pump following a similar approach adopted by Smith and Crampin (7) in developing a thermodynamically consistent model of the Na^{+}/K^{+} pump.

The SERCA pump is a P-type ATPase enzyme found in all muscle cells, and functions to sequester Ca^{2+} into the sarcoplasmic reticulum (SR) to facilitate muscle relaxation. A number of different SERCA isoforms exist, and their expression is dependent on the muscle type. SERCA1a is expressed in fast twitch skeletal muscle whereas SERCA2a is found slow twitch and cardiac muscle (8). These two SERCA isoforms are functionally identical, except that in the native cardiac SR environment, SERCA2a is regulated by phospholamban. The major function of the cardiac SERCA-ATPase is to keep the cytosolic Ca^{2+} concentration low by pumping Ca^{2+} into the SR and maintaining a Ca^{2+} concentration gradient across the SR membrane that is approximately three orders of magnitude in size during diastole. During Ca^{2+}-induced Ca^{2+} release, Ca^{2+} released from the SR increases the cytosolic Ca^{2+} concentration by an order of magnitude, which activates the contractile machinery and initiates muscle contraction. Muscle relaxation is then brought about by removal of Ca^{2+} from the cytosol which, under normal conditions, also results in restoration of the Ca^{2+} gradient across the SR membrane by the SERCA pump thereby preparing the cardiac myocyte for the next cardiac cycle. The SERCA pump is able to translocate Ca^{2+} against the concentration gradient by coupling the vectorial transport of Ca^{2+} across the SR membrane to the utilization of chemical energy via the hydrolysis of ATP. Two Ca^{2+} are translocated for each ATP that is hydrolyzed (9) according to the reaction

$$2Ca_i^{2+} + MgATP + H_2O \rightleftharpoons 2Ca_{sr}^{2+} + MgADP + Pi + H^{+}. \quad (1)$$

This reaction is fully reversible. The reversal condition depends on the relationship between the free energy of ATP hydrolysis and the energy required to transport Ca^{2+} against the concentration gradient (outlined in Methods, below).

Currently, there are no suitable biophysically based models of the cardiac SERCA pump that can be integrated into whole-cell and tissue frameworks for the purposes of simulating compromised metabolism. This is because

Submitted July 10, 2008, and accepted for publication November 5, 2008.

*Correspondence: k.tran@auckland.ac.nz or e.crampin@auckland.ac.nz

Editor: Herbert Levine.

0006-3495/09/03/2029/14 $2.00

doi: 10.1016/j.bpj.2008.11.045

existing models are not designed to be energetically sensitive and consistent with the fundamental principles of free energy transduction, or else they are simply too complex and computationally demanding. The most popular and simplest class of SERCA models is the phenomenologically based Michaelis-Menten description which typically involves three parameters: a K_m; a cooperativity term, n; and a V_{max}. These models depend solely on the cytosolic Ca^{2+} concentration and, due to their simplicity and computational efficiency, are often employed in whole-cell modeling frameworks that include descriptions of Ca^{2+} handling dynamics (Ca^{2+}-induced Ca^{2+} release). A refinement to these models is a reversible model of the cardiac SERCA pump whose flux is a function of cytosolic and luminal Ca^{2+} concentrations (10). The model specifies a fixed physiological Ca^{2+} gradient across the SR membrane at normal physiological conditions, at odds with the thermodynamic requirement that this gradient should vary as a function of the free energy available from ATP hydrolysis and energy loss from Ca^{2+} leak. More-complex models typically focus on capturing, with varying success, the large number of partial reactions that make up the SERCA cycle. This is brought about by the complex interactions between the SERCA pump and various ionic species present in the cytosol (namely, Mg^{2+}, K^+, and H^+) as well as its interaction with the metabolites MgATP, MgADP, and Pi. These models tend to be highly complex in terms of their structure and contain a large number of state variables and parameters. Examples of such models include those of Gould et al. (11) and Haynes and Mandveno (12). While they are highly detailed in terms of mechanism, their complex nature renders them unsuitable for whole-cell and tissue simulations.

Here we present a mathematical model of the cardiac SERCA pump that consolidates a variety of experimental data, collected from a range of modalities, and the fundamental principles of free energy transduction into a consistent single framework. We aim to develop a model of the SERCA pump in its native cardiac environment where it is intrinsically under the regulation of phospholamban. We employ a lumping scheme for rapid equilibrium partial reactions to simplify and reduce the number of model parameters, and simultaneously fit the model to a collection of experimental data that capture the dependence of the SERCA pump on Ca^{2+}, H^+, MgATP, MgADP, and Pi. This model enables integration of the SERCA function into whole-cell ventricular myocyte and continuum-based tissue models to simulate the effects on Ca^{2+} dynamics when cellular metabolism is compromised.

METHODS

The kinetic model is based on the E1-E2 model for Ca^{2+} transport (13,14) with the addition of H^+ binding steps (Fig. 83 of Bers (8)) to capture the pH dependence of the pump (Fig. 1). When the pump operates in the forward (clockwise) direction, two Ca^{2+} are bound from the cytoplasm and released into the SR lumen. This cycling is driven by the binding and hydrolysis of MgATP, followed by the release of the products MgADP, Pi, and a H^+. The model has a total of 12 states, which is reduced to three states based on rapid equilibrium assumptions surrounding the ion binding steps. The model is solved as a steady-state solution and the parameters are simultaneously fitted to a diverse set of data that characterize the ionic and metabolic properties of the cardiac SERCA pump.

Ca^{2+} binding mechanism

In the E1-E2 model, the SERCA pump is assumed to have two Ca^{2+} binding sites with affinities for Ca^{2+} that depend on their orientations. When the binding sites are facing the cytosol, their affinity for Ca^{2+} is much higher than when they are facing the SR lumen, facilitating the binding, transport and subsequent release of Ca^{2+} into the SR. Experiments using radioactively-labeled Ca^{2+} have found that the Ca^{2+}-binding sites bind Ca^{2+} in a sequential manner (15–19) and lead to the theorized existence of a narrow channel that consists of a deep and a superficial binding site (20). Moreover, the binding of the first Ca^{2+} into the deep site is followed by development of a higher binding affinity to the second superficial site, characterizing a positive cooperative binding mechanism (21). This sequential behavior is represented in the reaction scheme in Fig. 1 by the binding of Ca^{2+} between states P2 and P4. The second Ca^{2+} can bind only after the first Ca^{2+} has bound.

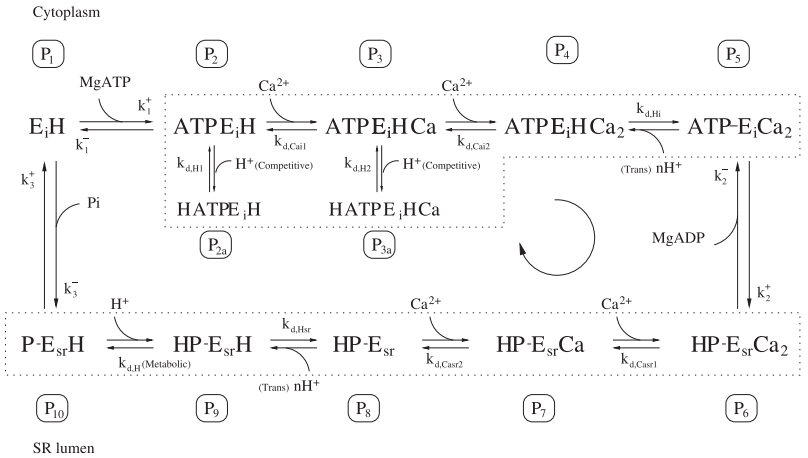

FIGURE 1 Schematic of the 12-state cardiac SERCA pump model. The binding of Ca^{2+} from both the cytosol and SR lumen is modeled as a partially cooperative mechanism with different K_d values for the first and second Ca^{2+} binding. There are five H^+ binding events in the model: two for the competitive binding of H^+ to the Ca^{2+}-binding sites, two for the binding of H^+ involved in the Ca^{2+}/H^+ counter-transport, and one for the release of the metabolic H^+. The boxed Ps denote the probability of being in a particular state. The conformation change from E1 to E2 and back again occurs between states P5 and P6 (concomitant with ADP release), and P10 and P1 (concomitant with Pi release), respectively. For each cycle in the clockwise (forward) direction, the pump transports two Ca^{2+} for each ATP that is hydrolyzed. The dotted boxes indicate the partial reactions (ion binding) that are assumed to be rapid equilibrium steps (see Model Simplification: Rapid Equilibrium Assumptions). The subscripts *i* and *sr* are equivalent to 1 and 2 in the E1-E2 notation, respectively.

The cooperative binding mechanism can be classified as being partially or fully cooperative. Cooperative binding can be represented mathematically by setting different binding constants for the first and second Ca^{2+} binding sites; partially cooperative binding is represented by a larger second Ca^{2+}-binding constant while fully cooperative binding is represented by an instantaneous binding of the second Ca^{2+}. In the case of fully cooperative binding, only one set of binding constants is necessary to characterize the reaction. A similar sequential and cooperative binding mechanism is also assumed when the binding sites orient themselves to face the SR lumen (19). We compare how well the SERCA model fits the data when the Ca^{2+}-binding mechanism is modeled either as a partially cooperative binding scheme (Fig. 1) or as a fully cooperative binding scheme (Fig 2).

Ca^{2+}/H^+ counter-transport

The ejection of H^+ from SR vesicles after the addition of Ca^{2+} and ATP has been observed by a number of experimental groups (22–24). The extent of the ejection is greater than can be accounted for by H^+ production arising from ATP hydrolysis and is due to the counter-transport of H^+ for Ca^{2+}. A number of experimental groups have measured the stoichiometry to be 2:2 where 2 H^+ are exchanged for 2 Ca^{2+} during each SERCA cycle at neutral pH (24,25). We incorporated this exchange of H^+ into our model by assuming distinct H^+ binding sites on the SERCA enzyme (between states P4 and P5 and states P8 and P9 in Fig. 1). The binding of H^+ to SERCA, when the Ca^{2+}-binding sites are facing the cytosol, has been placed between states P8 and P9, following titration experiments that have shown the ejection of H^+ into the cytosol to occur after the binding of Ca^{2+} to the high affinity Ca^{2+}-binding sites (23). The binding of H^+ on the luminal side is assumed to be after the release of Ca^{2+}. The stoichiometry of H^+ binding in the SERCA model was left as an adjustable parameter in the fitting process as it has been suggested that the number of H^+ extruded per cycle depends on pH (26). The native SR vesicle membrane is highly permeable to H^+ and other monovalent ions, and abolishes the formation of any steady-state H^+ gradient (27). Hence, the H^+ concentration is assumed to be the same inside and outside of the SR.

Competitive H^+ binding

Protons also directly compete with Ca^{2+} in binding to the two Ca^{2+} -binding sites on the SERCA enzyme (19). At decreasing pH levels, there is a progressive increase in the K_m for the Ca^{2+} dose-response curve (28). This is modeled as a side reaction at states P2 and P3 of Fig. 1, where the enzyme can bind either Ca^{2+} or H^+. In the model, the competitive H^+ binding mechanism exists only when the Ca^{2+}-binding sites are facing the cytosol and is not included for the case when they face the SR lumen. Whether this is sufficient to capture the pH-dependent data from Ji et al. (28) is investigated below.

Metabolite binding

When the pump is cycling in the forward direction, MgATP initially binds and phosphorylates the SERCA enzyme (29). This results in a slow conformational change in which the cytosol-facing Ca^{2+}-binding sites now orient themselves to face the SR lumen and at the same time bring about a large decrease in Ca^{2+}-binding affinity (13,14,27). Concomitant with the slow conformational change is a rapid dissociation of MgADP (30). This is followed by release of the other two hydrolysis products, the metabolic H^+ and Pi, which is accompanied by a second conformational change that restores the Ca^{2+}-binding sites back to their cytosol-facing orientation. The binding/unbinding of the metabolites MgATP, MgADP, and Pi along with the metabolic proton are all modeled as individual partial reactions. The MgADP dissociation step (between states P5 and P6), however, also encompasses the phosphorylation and subsequent conformational change of the enzyme, while the Pi dissociation step (between states P10 and P1) encompasses the second conformational change. In the model, MgATP binding is placed before binding of the first Ca^{2+}. However, experimental literature suggests that Ca^{2+} can bind in both the presence and absence of MgATP (21,31). This implies that there may be two distinct MgATP and Ca^{2+} binding sites that can bind the ligands in any order. To investigate this, we have compared fitted models where MgATP binds before or after Ca^{2+} binding.

Thermodynamic constraints

The coupling of free energy available from the hydrolysis of ATP (ΔG_{MgATP}) to the transport of Ca^{2+} into the SR lumen by the SERCA enzyme against a concentration gradient (ΔG_{SERCA}) imposes a constraint on the system. This constraint determines the direction of the pump when the myocyte is metabolically compromised. Thermodynamic constraints are incorporated into the SERCA model following the techniques outlined in Smith and Crampin (7). Briefly, the free energy of ATP hydrolysis depends on the ratio of MgATP to its hydrolysis products as

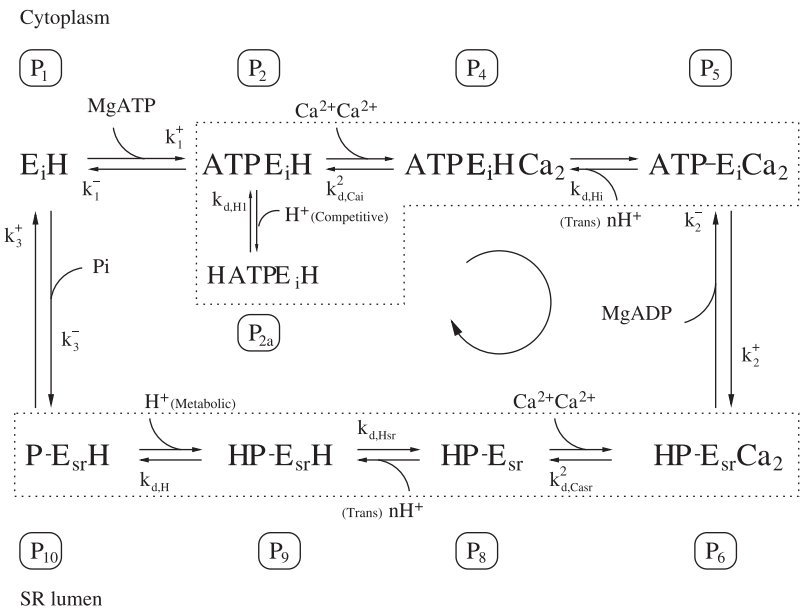

FIGURE 2 Schematic of cardiac SERCA model where the Ca^{2+} binding mechanism is assumed to be fully cooperative. States P3 and P3a no longer exist as they quickly evolve into P4 from the binding of the second Ca^{2+}. Similarly in the SR lumen, state P7 has evolved into P6.

$$\Delta G_{\mathrm{MgATP}} = \Delta G^{\mathrm{o}}_{\mathrm{MgATP}} + RT\ln\frac{[\mathrm{MgADP}][\mathrm{Pi}][\mathrm{H}^+]}{[\mathrm{MgATP}]}, \quad (2)$$

where T is the temperature, R is the universal gas constant, and $\Delta G^{\mathrm{o}}{}_{\mathrm{MgATP}}$ is the free energy under standard conditions and is defined as $\Delta G^{\mathrm{o}}{}_{\mathrm{MgATP}} = -RT\ln K_{\mathrm{MgATP}}$ ($\Delta G^{\mathrm{o}}{}_{\mathrm{MgATP}} = 11.9$ kJ mol^{-1}, taking [H$^+$] into account). The energy required to move two Ca^{2+} against a concentration gradient is given by

$$\Delta G_{\mathrm{SERCA}} = 2RT\ln\frac{[\mathrm{Ca}^{2+}]_{\mathrm{sr}}}{[\mathrm{Ca}^{2+}]_{\mathrm{i}}}. \quad (3)$$

The SERCA pump will cycle in the forward direction when $\Delta G_{\mathrm{MgATP}} + \Delta G_{\mathrm{SERCA}} < 0$, as is the case under normal physiological conditions and Ca^{2+} will be transported back into the SR, thereby allowing the muscle to relax. When the free energy of ATP hydrolysis drops, or when the Ca^{2+} gradient across the SR membrane changes such that the net free energy becomes zero, the pump will stop and cease to transport any more Ca^{2+}. Should the free energy of ATP hydrolysis drop further, and the net free energy become positive, the pump will cycle in the reverse direction and generate ATP from ADP and Pi using the energy stored in the Ca^{2+} concentration gradient across the SR membrane. The thermodynamic considerations here indicate the point at which the pump reverses. The rate at which the pump cycles, however, is determined purely by the kinetic parameters of the model. Detailed balance enforces a further constraint on the kinetic parameters of the scheme in Fig. 1 (32). The product of the forward transition rates in the model is equal to the product of reverse transition rates

$$\prod_{\mathrm{i}=1}^{n} k_{\mathrm{i}}^{+} P_{\mathrm{i}} = \prod_{\mathrm{i}=1}^{n} k_{\mathrm{i}}^{-} P_{\mathrm{i}+1}, \quad (4)$$

where P_{i} and $P_{\mathrm{i}+1}$ are the fractional occupancies of adjacent states, and $k_{\mathrm{i}}{}^{\pm}$ are rate constants of first order. If the transition involves the binding or unbinding of an ion, the expression is written explicitly in terms of the ion concentration and a rate constant of higher order, $k_{\mathrm{i}}{}^{+}[\mathrm{Y}]P_{\mathrm{i}} = k_{\mathrm{i}}{}^{-}P_{\mathrm{i}+1}$, where [Y] is an ion concentration. The fractional state occupancies cancel out in Eq. 4, leaving a constraint on the kinetic parameters which must hold whether or not the system is in equilibrium. Applying this to the SERCA scheme in Fig. 1 gives

$$\frac{k_1^+ k_2^+ k_3^+ K_{\mathrm{d,Casr1}} K_{\mathrm{d,Casr2}} K_{\mathrm{d,Hsr}} K_{\mathrm{d,H}}}{k_1^- k_2^- k_3^- K_{\mathrm{d,Cai1}} K_{\mathrm{d,Cai2}} K_{\mathrm{d,Hi}}} = \frac{[\mathrm{MgADP}][\mathrm{Pi}][\mathrm{H}^+][\mathrm{Ca}^{2+}]_{\mathrm{sr}}^2}{[\mathrm{MgATP}][\mathrm{Ca}^{2+}]_{\mathrm{i}}^2}. \quad (5)$$

Substituting Eqs. 2 and 3 into the equilibrium expression,

$$\Delta G_{\mathrm{MgATP}} + \Delta G_{\mathrm{SERCA}} = 0,$$

gives

$$\Delta G^{\mathrm{o}}_{\mathrm{MgATP}} + RT\ln\frac{[\mathrm{MgADP}][\mathrm{Pi}][\mathrm{H}^+]}{[\mathrm{MgATP}]} + 2RT\ln\frac{[\mathrm{Ca}^{2+}]_{\mathrm{sr}}}{[\mathrm{Ca}^{2+}]_{\mathrm{i}}} = 0 \quad (6)$$

$$RT\ln\frac{[\mathrm{MgADP}][\mathrm{Pi}][\mathrm{H}^+][\mathrm{Ca}^{2+}]_{\mathrm{sr}}^2}{[\mathrm{MgATP}][\mathrm{Ca}^{2+}]_{\mathrm{i}}^2} = \Delta G^{\mathrm{o}}_{\mathrm{MgATP}},$$

and substituting the left-hand side of Eq. 6 with the right-hand side of Eq. 5 yields a constraint on the kinetic rate constants of the SERCA pump model,

$$\frac{k_1^+ k_2^+ k_3^+ K_{\mathrm{d,Casr1}} K_{\mathrm{d,Casr2}} K_{\mathrm{d,Hsr}} K_{\mathrm{d,H}}}{k_1^- k_2^- k_3^- K_{\mathrm{d,Cai1}} K_{\mathrm{d,Cai2}} K_{\mathrm{d,Hi}}} = e^{\Delta G^{\mathrm{o}}_{\mathrm{MgATP}}/RT}. \quad (7)$$

Model simplification: rapid equilibrium assumptions

It is assumed in the model that the ionic reactions (binding of Ca^{2+} and H^+) occur at a faster rate than the reactions involving the metabolites. A number of groups have proposed that Ca^{2+} binding is comprised of fast binding of the first Ca^{2+}, followed by a slow conformational change that allows binding of the second Ca^{2+} (15,21). However, more recently, Tanford et al. (33) have proposed a sequential Ca^{2+} binding model, where the conformational change after binding of the first Ca^{2+} is assumed to be minor (compared to the E1-E2 conformation change) based on work by MacLennan et al. (34) and Brandl (35) on the structure of the SERCA enzyme. We have therefore assumed the entire Ca^{2+} binding process for both the cytosol and lumen-facing orientations to equilibrate rapidly in comparison to the E1-E2 conformation changes.

The assumption that the MgADP and Pi partial reactions are slow is justified on the basis that those reactions also encompass a change in the SERCA enzyme conformation, which is typically a relatively slow process (36). The MgATP reaction is also modeled as a slow process because MgATP binding has been shown to be rate-limiting at very low concentrations (20).

Application of the rapid equilibrium assumption to the partial reactions follows the technique outlined in Smith and Crampin (7). This results in a simplified three-state model, where apparent rate constants replace the forward and backward rate constants for the ionic partial reaction steps (Fig. 3). The apparent rate constants are given in the Appendix and are functions of ionic concentrations and dissociation constants for the rapid ionic reactions. The number of parameters is reduced from 24 in the 12-state model to 12 in the three-state model.

The SERCA pump is assumed to be operating at a kinetic steady state in the context of a whole-cell simulation. This quasi-steady-state approximation assumes that the conformational changes of the enzyme (between states P5 and P6, and P10 and P1 in Fig. 1) are rapid compared to slower processes in the cell such as changes in ionic concentrations. The steady-state flux of the cycle is solved using the diagram method (32) and the clockwise cycle rate per pump at steady state is given by

$$\nu_{\mathrm{cycle}} = \frac{\alpha_1^+ \alpha_2^+ \alpha_3^+ - \alpha_1^- \alpha_2^- \alpha_3^-}{\Sigma_3}. \quad (8)$$

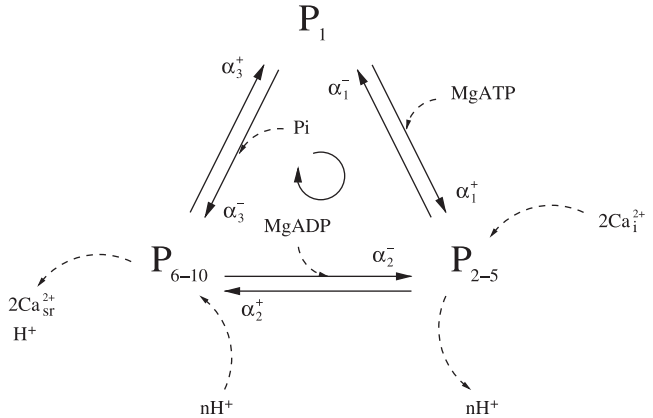

FIGURE 3 Schematic of the simplified three-state model. Application of the rapid equilibrium assumption to the ion-binding partial reactions (states within the *two dotted boxes* in Fig. 1) results in a simplified three-state model. The apparent rate constants ($\alpha_{\mathrm{i}}{}^{\pm}$, $i = 1, 2, 3$) replace the forward and backward rate constants and are a function of ion concentrations and dissociation constants.

in units of s^{-1}, where Σ_3 is a sum of nine positive product terms given in the Appendix. For integration into a cell model, the whole-cell pump flux will be given by

$$J_{SERCA} = 2\ \nu_{cycle}\ \rho_{sr}\ A_{sr}, \quad (9)$$

where ρ_{sr} is the density of the SERCA pumps per unit area of membrane, A_{sr} is the surface area of the SR membrane, and the stoichiometric constant is due to the transport of two Ca^{2+} per cycle. The Ca^{2+} flux, J_{SERCA}, has units of mol s^{-1}.

Data set to constrain parameters

To characterize quantitatively the parameters for the cardiac SERCA model, a set of data was chosen that captures the metabolic and ionic dependencies of the pump. The aim was to use whole pump flux data as a function of Ca^{2+}, H^+, and each of the metabolites and, where possible, data that are derived from native cardiac SERCA preparations to capture the intrinsic influence of phospholamban on the Ca^{2+}-sensitivity curve (which shifts to the right in the presence of phospholamban). This is achieved through the incorporation of Ca^{2+}-dependent data from Ji et al. (28), which are derived from cardiac microsomes. Table 1 details the conditions for each of the data sets. Without reliable data on the Q_{10} values of the various steps in the SERCA cycle, we have chosen to correct for the differences in temperature between the data sets by normalizing the data. The entire data set was normalized to a maximum cycle rate of 5 s^{-1} at optimal conditions, defined as $[Ca^{2+}]_{sr} = 0$, $[Ca^{2+}]_i = 10\ \mu M$, [ATP] = 5 mM, [ADP] = 0, [Pi] = 0, and pH = 7.2. These values were chosen based on a maximal flux value of 4.2 s^{-1} obtained from intact rabbit myocytes obtained at 22°C (37). Maximal flux values from canine and guinea pig ventricular myocytes have been estimated to be between 5 s^{-1} at 25°C and 7.5 s^{-1} at 37°C, respectively (8,38,39). Details of the data used in the parameter optimization are outlined in Table 1.

Parameter optimization

The parameters in the three-state model were estimated using the particle swarm optimization method. This is a population-based approach that scatters a set of solution particles into the parameter space. Each particle moves through the space with a velocity that depends on the best solution so far encountered by that particle and the best solution encountered by any particle in the swarm (40). The solutions obtained from the particle swarm optimization method were then used as initial conditions in a Levenberg-Marquardt least-squares fitting procedure to refine the solution. The fitting process was written and carried out in MatLab (The MathWorks, Natick, MA).

RESULTS

Ca^{2+} binding

Ca^{2+} binding is assumed to be either partially cooperative or fully cooperative, both with a stoichiometry of two Ca^{2+} translocated per ATP hydrolyzed. We sought to compare these two hypotheses by fitting the data to a fully cooperative model (Fig. 2) and a partially cooperative model (Fig. 1). There are three fewer parameters in the fully cooperative model (removal of two parameters for Ca^{2+} binding in the cytosol and lumen-facing orientations, and one from the second competitive H^+ binding). We find that there is no discernible difference between the results of the two models (difference of residuals of 3%). Fig. 4 shows the fit achieved with the fully cooperative Ca^{2+} binding model. The fully cooperative Ca^{2+} binding model is favored over the partially cooperative Ca^{2+} binding model as it achieves a similar quality of fit while using three fewer parameters. The fitting of data in the remainder of the results below was achieved using the fully cooperative Ca^{2+} binding model. The optimized parameters for the model are given in Table 2. Fig. 4 shows that the SERCA flux is a sigmoidal function of cytosolic pCa. This sigmoidal function is pH-dependent and shifts progressively to the right (increase in K_m) as pH is decreased. This is due to the competitive binding of H^+ to the Ca^{2+}-binding site when both are facing the cytosol. Note that H^+ binding competitively to the cytosol-facing Ca^{2+}-binding site, alone, is required to achieve this fit, suggesting that competitive binding of H^+ on the luminal side is not required to fit this set of data. Also, at a normal pH of 7, the K_m for the flux-Ca^{2+} curve is 0.26 μM—similar to parameters employed in a reversible SERCA model (10).

TABLE 2 Parameters for the three-state SERCA model generated from the optimization process

Parameter	Value
k_1^+	25,900 $mM^{-1}\ s^{-1}$
k_2^+	2540 s^{-1}
k_3^+	20.5 s^{-1}
k_1^-	2 $mM^{-1}\ s^{-1}$*
k_2^-	67,200 $mM^{-1}\ s^{-1}$
k_3^-	149 $mM^{-1}\ s^{-1}$
$K_{d,Cai}$	0.91 mM
$K_{d,Casr}$	2.24 mM
$K_{d,H1}$	1.09×10^{-5} mM
$K_{d,Hi}$	3.54×10^{-3} mM^2
$K_{d,Hsr}$	1.05×10^{-8} mM^2
$K_{d,H}$	7.24×10^{-5} mM
n	2.0

*k_1^- is constrained by detailed balance (see Methods) and is dependent on the kinetic and dissociation constants of the model (see Appendix).

TABLE 1 Description of the data used to constrain the parameters in the three-state model

Species and preparation	Data	T	pH	ATP	ADP	Pi	$[Ca^{s+}]_i$	$[Ca^{s+}]_{sr}$	Reference
Mouse SERCA2a cardiac microsomes	Ca^{2+} uptake versus pH (Fig. 5)	37	*	3	0	0	0	0.001	(28)
Mouse SERCA2a cardiac microsomes	Ca^{2+} uptake versus $[Ca^{2+}]_i$ at different pH (Fig. 4)	37	*	3	0	0	*	0	(28)
Rabbit SERCA1a nonnative cell expression	Level of back phosphorylation versus [Pi] (Fig. 6)	25	6	0	0	*	0	0	(41)
Rabbit SERCA1a solubilized SR fragments	ATPase activity vesus ATP and ADP (Fig. 7)	10	7	*	*	0	5	5	(42)

The units of [ATP], [ADP], [Pi], $[Ca^{s+}]_i$, and $[Ca^{s+}]_{sr}$ are in mM and temperature, T, is in °C.
*Dependent variable used in the fitting process.

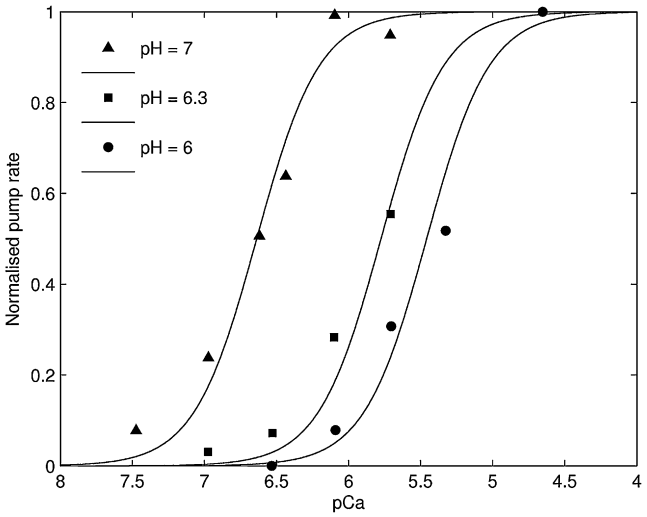

FIGURE 4 The fit of the three-state model with fully cooperative Ca^{2+} binding (Fig. 2) to the pH-dependent Ca^{2+} binding data from Ji et al. (28).

Ca^{2+}/ H^+ countertransport

The SERCA pump flux exhibits a bell-shape dependence on pH. The pump operates optimally at a pH of ~7.1 (Fig. 5). The bell-shaped curve results from the product of two opposing Hill-type relationships arising from the four H^+ binding events in the model. Two of the H^+-binding events are from the Ca^{2+}/H^+ counter-transport mechanism, one from the metabolic reaction and the other from the competition with Ca^{2+} for the Ca^{2+}-binding sites. The stoichiometry for the H^+ binding involved in the Ca^{2+}/ H^+ counter-transport was treated as a parameter in the optimization process. The optimal fit produced a value of 2.0, which is consistent with experimental observations of 2 (24,25). This stoichiometric relation governs the narrowness of the bell-shape relationship.

Metabolite dependence

The Pi dependence of the SERCA pump is captured from data that measured the relative proportion of the enzyme that is in a phosphorylated state brought about by the addition of varying concentrations of Pi (41). The data shows that when the Pi concentration is in the mM range, almost all the SERCA enzymes are in the phosphorylated state. In the model, state P_{6-10} in Fig. 3 is assumed to be the phosphorylated states and the results of the optimization give a good fit to the data (Fig. 6).

Dependence of the SERCA model on MgATP and MgADP concentrations is quantified by fitting to data from Sakamoto and Tonomura (42). The SERCA pump flux increases with increasing MgATP concentration and reaches a saturating flux that is dependent on the MgADP concentration (Fig. 7).

There is evidence in the literature showing MgATP to bind both before and after the binding of Ca^{2+} in the cytosol-facing orientation. To investigate this disparity, we fitted a model where MgATP binds before Ca^{2+} binding (Fig. 1) and compared it to a model where MgATP was placed immediately after Ca^{2+} binding. We found that when the MgATP was placed after the binding of the second Ca^{2+}, a reasonable fit could not be achieved compared with the model where the MgATP was placed before the first binding Ca^{2+} (Fig. 7). The same result was observed when the MgATP binding step was placed after the dissociation of the H^+ on the cytosolic side. This suggests that MgATP binds first, followed by Ca^{2+} and H^+. To minimize the risk of missing the optimal parameter set, we took the following strategy: a large number of runs (>100) with random starting points was carried out in each case. The starting points for the parameters were within defined boundaries which were set to be the same as those in the successful fit. These boundaries were also increased but no satisfactory fit was produced. Based on this result, it

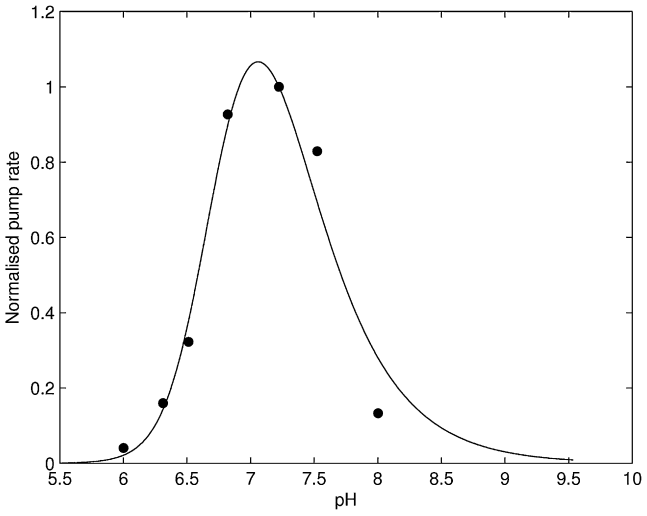

FIGURE 5 The fit of the three-state model with fully cooperative Ca^{2+} binding (Fig. 2) to pH data from Ji et al. (28).

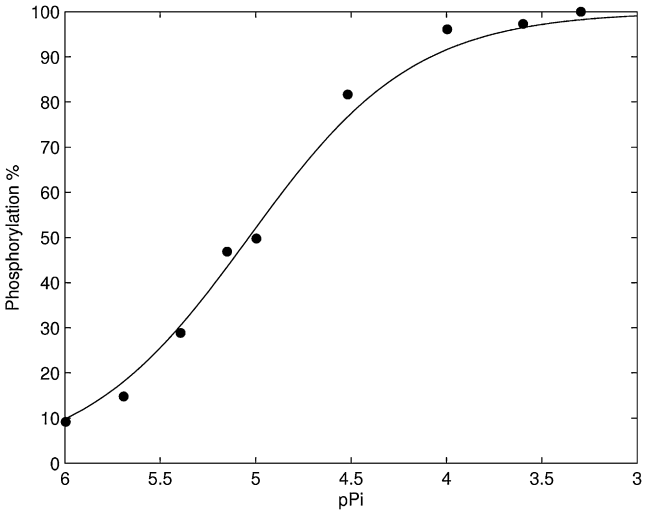

FIGURE 6 The fit of the three-state model with fully cooperative Ca^{2+} binding (Fig. 2) to Pi phosphorylation data from Dode et al. (41).

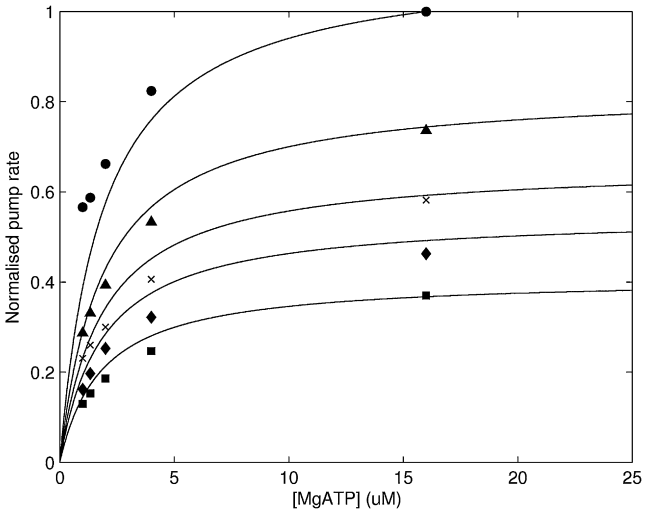

FIGURE 7 The fit of the three-state model with fully cooperative Ca^{2+} binding (Fig. 2) to ATP and ADP-dependence data from Sakamoto and Tonomura (42). Descending from the top curve, the ADP concentrations are 0 mM, 20 mM, 40 mM, 60 mM, and 100 mM.

was concluded that only a model with the MgATP binding site placed before binding of the first Ca^{2+} can produce an adequate fit to the data set.

Thermodynamic properties of the model

The thermodynamic properties of the pump are demonstrated by investigating the relationship between the free energy of ATP hydrolysis and the SERCA cycle flux at different levels of luminal Ca^{2+} concentration (Fig. 8). The free energy of ATP hydrolysis is progressively reduced by increasing the concentration of Pi. The pump stops completely at the reversal point where the net free energy is zero; i.e., the energy required by the pump to transfer Ca^{2+} into the SR is equal to the available free energy. Furthermore, when the energy in the Ca^{2+} gradient exceeds the available free energy, the model predicts a reversal of the pump where ATP is generated from ADP and Pi. The rate at which the pump operates in reverse is determined by the kinetic parameters of the model. Fig. 9 shows the effect of increasing MgADP, rather than Pi, to progressively reduce the available free energy. The cycle still reverses as net free energy goes through zero, but in this case, an increase in MgADP brings about a negligible reversal rate. Analysis of the three-state model reveals that for large values of MgADP, the maximal reverse rate is equal to $\frac{\alpha_1^- \alpha_3^-}{\alpha_1^+ + \alpha_1^- + \alpha_3^-}$. Under normal Ca^{2+} and pH conditions, this expression is dominated by the magnitude of α_1^+, the forward rate of MgATP binding, which renders the maximal reverse flux negligible as MgADP is increased (Fig. 9). This is because as MgADP tends to very large values, state P_{2-5} (Fig. 3) becomes saturated and progression to state P_1 is restricted by the large binding constant of MgATP. A similar analysis for increasing Pi concentration shows that as Pi is greatly increased, the maximal reverse rate is equal to $\frac{\alpha_1^- \alpha_2^-}{\alpha_1^- + \alpha_2^- + \alpha_2^+}$. The maximal reverse rate for [Pi] is therefore independent of the kinetics of MgATP binding and depends, instead, on the combined effects of Ca^{2+}, pH, and MgADP. Increases in Pi can therefore overcome the inhibition of the large MgATP binding constant, as shown

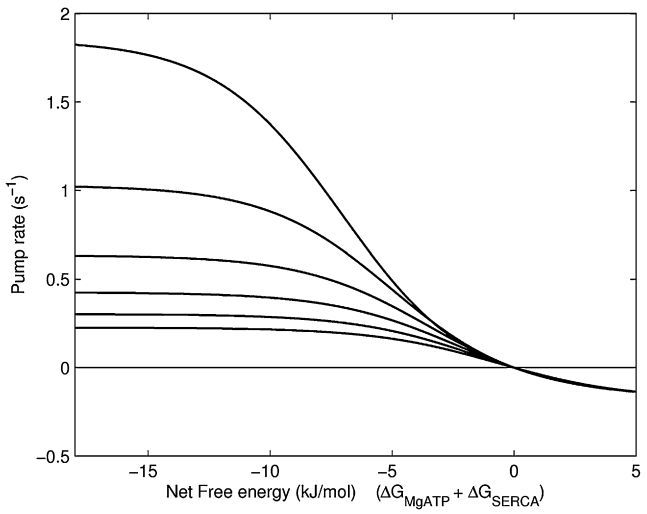

FIGURE 8 The effect of changes in the net free energy on the cycle pump rate at different luminal Ca^{2+} concentrations. The top curve is at $[Ca^{2+}]_{sr}$ = 1 mM, increasing by 0.5 mM for each curve up to 3.5 mM for the lowest curve. The free energy of ATP hydrolysis is reduced by increasing [Pi]. Other conditions in the simulation: ATP = 5 mM, ADP = 36.3 μM, pH = 7, $[Ca^{2+}]_i$ = 1 μM.

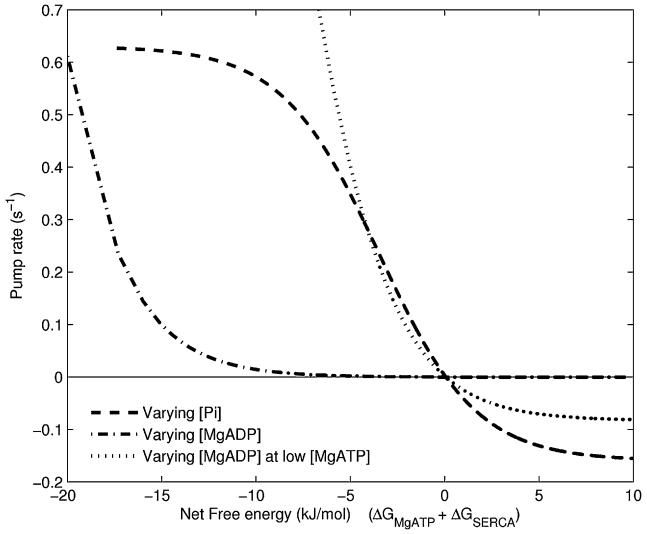

FIGURE 9 The SERCA model predicts a reversal point when the net free energy is zero. However, the rate at which the pump reverses is a function of the model parameters. In the figure above, the free energy of ATP hydrolysis is reduced by increasing either [Pi] or [MgADP]. Increasing [Pi] causes the pump to reverse at an appreciable rate beyond the reversal point. However, increasing [MgADP] results in the pump slowing down considerably as it passes through the reversal point. [MgATP] = 5 mM for both curves. But when [MgADP] is increased while keeping [MgATP] low (10 μM), there is an appreciable reversal rate because the inhibitory effect of MgATP binding is reduced. Other conditions in the simulation: pH = 7, $[Ca^{2+}]_i$ = 1 μM, $[Ca^{2+}]_{sr}$ = 2 mM.

in Fig. 9, but to do so requires a very large and nonphysiological Pi concentration. The kinetics of MgATP binding therefore limits the maximum reversal rate of the pump. When the pump rate is plotted at a lower MgATP concentration, there is an appreciably larger reversal rate because the inhibitory effect of MgATP binding has been reduced.

Simplifying to a two-state model

For physiological concentrations of metabolites, the three-state model can be further simplified by noting that the MgATP concentration in the Sakamoto and Tonomura (42) data set is in the μM range. The MgATP binding was defined as a slow step to capture these data. These low MgATP concentrations, however, are outside the physiological range: normal MgATP concentration in a healthy myocyte is ~5 mM while, during ischemia, the MgATP concentration drops by ~50% over the 15 min after the initial ischemic insult (43). Therefore, under physiological and even ischemic conditions, the binding of MgATP can be considered to be a rapid equilibrium reaction and, as such, the SERCA model can be further simplified to a two-state model.

Using rapid equilibrium assumptions, the slow MgATP binding step is turned into a rapid binding step (Fig. 10) by lumping the kinetic constants, k_1^+ and k_1^-, into a single dissociation constant, $K_{d,ATP}$, where $K_{d,ATP} = k_1^-/k_1^+$. This results in a two-state model (Fig. 11) where the MgATP binding step joins the cytosol-facing Ca^{2+} binding steps in a single state. In the limit when MgATP concentration is in the mM range, the two-state model behaves essentially the same as the three-state model. Fig. 12 shows a simulation comparing the two- and three-state models. It demonstrates that the two models are essentially identical when MgATP is in the mM range but begin to diverge when MgATP drops to the μM range.

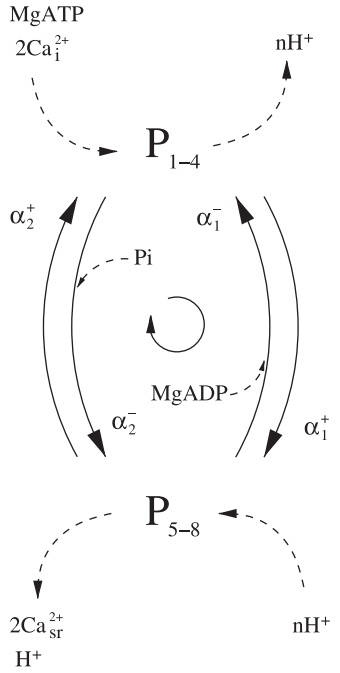

FIGURE 11 Application of the rapid equilibrium assumption to the ATP binding step reduces the three-state model further to a two-state model. The releases of ADP and Pi are assumed to be concomitant with the conformational change of the SERCA enzyme from the E1 to E2 state and are therefore modeled as relatively slower reactions. Equations for the two-state model are given in the Appendix.

DISCUSSION

Active energy-demanding processes play key roles in all cell types by converting chemical energy in the form of ATP into useful work. In a cardiac myocyte, the major energy-demanding processes, whose functions depend critically on the cellular energetic state, are the Na^+/K^+ pump, the SERCA pump, and acto-myosin ATPase. The two pumps, in particular, are integral components of electrophysiological modeling frameworks that encompass Ca^{2+} handling dynamics (2–6). However, the omission of metabolic sensitivity in modeling these processes leads to difficulties when attempting to simulate conditions where the energetic state of a myocyte is compromised such as would be encountered during an ischemic episode (43). Recently, an energy-

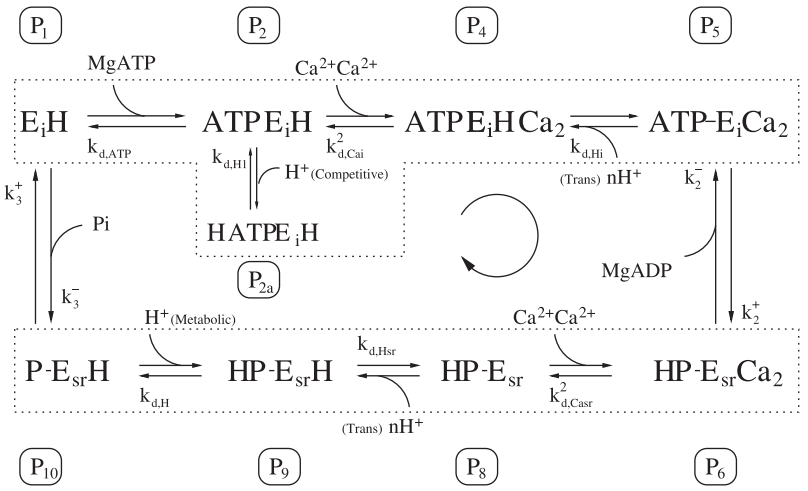

FIGURE 10 Application of the rapid equilibrium assumption to the ATP binding step reduces the forward and back binding constants (between states P1 and P2) to a single dissociation constant, $K_{d,ATP}$. The ATP binding step becomes lumped with the Ca^{2+} and H^+ binding steps as outlined by the top dotted box.

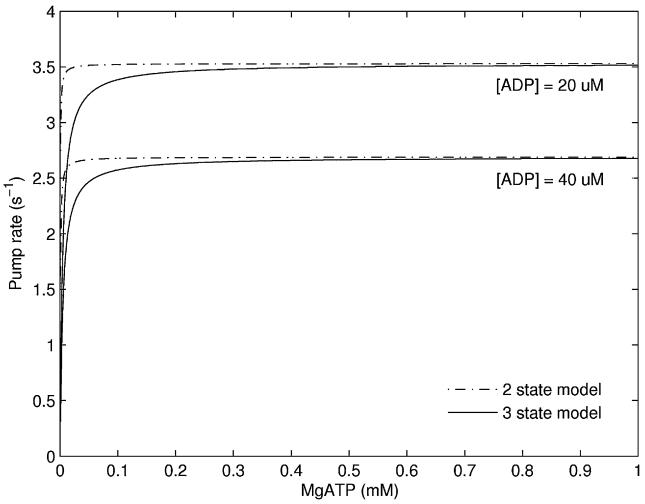

FIGURE 12 Simulations comparing the two- and three-state models show that they are identical when the ATP concentration is in the μM range. Conditions for simulation: pH = 7, $[Ca^{2+}]_i$ = 1 μM, $[Ca^{2+}]_{sr}$ = 1 mM, Pi = 1 mM.

sensitive model of the cardiac Na^+/K^+ pump has been published (7,44) and used to investigate the role of the pump during ischemia. Using the approach outlined in Smith and Crampin (7), we have developed a mathematical model of the cardiac SERCA pump, which is sensitive to the metabolic state of the cell as well as the luminal and cytosolic concentrations of Ca^{2+} and H^+. This model brings together a variety of experimental data under the framework of the biophysical E1-E2 model and enforces thermodynamic consistency by introducing a constraint on the rate constants of the model.

The analysis of the simplified model presented here does not necessarily prove that this model is unique. Rather, we have shown that this model is sufficient to describe a range of experimental data on the SERCA pump flux. Although we have ruled out several other kinetic schemes during the development of this model, there may be other kinetic schemes that, when simplified, produce similar fits to the data. Furthermore, as more data become available, these can be incorporated into an initially more complex scheme which can be subsequently simplified without loss of detail, using the method presented here.

SERCA is modeled initially as a 12-state cycle modified from de Meis and Vianna (14) to include aspects of H^+ binding. Two H^+ partial reactions are included to capture the Ca^{2+}/H^+ counter-transport, two more for the competitive binding to the Ca^{2+}-binding sites, and another to account for the metabolic H^+. This model is simplified based on the assumption that the reactions involving the binding/unbinding of Ca^{2+} and H^+ occur on a timescale that is significantly faster than the conformational change of the pump as it switches between the cytosol and lumen-facing configuration. The simplified model presented here does not explicitly represent all the possible intermediate states of the cardiac SERCA pump. However, the dependencies and ions represented by these intermediate states are retained in the transition rates between states of the simplified model, which are shown to be sufficient to characterize the pump's sensitivity to Ca^{2+} and H^+, and the metabolites, MgATP, MgADP, and Pi.

Ca^{2+} binding

Ca^{2+} is known to bind in a positive cooperative manner (21). We used our model to assess whether this binding is a partially cooperative mechanism or a fully cooperative mechanism. In the case of the partially cooperative mechanism, the binding constant of the second Ca^{2+} is greater than that of the first whereas in the fully cooperative case, the binding of the second Ca^{2+} is assumed to be instantaneous after the first Ca^{2+} binding to the pump. Mathematically, the fully cooperative mechanism has three fewer parameters. The results of fitting these two models to the data show negligible difference in residuals. The parsimonious approach therefore favors the fully cooperative mechanism over the partially cooperative mechanism, since, given the available data, it is impossible to distinguish between the two cases.

The Ca^{2+} binding characteristics of the model cannot be validated by directly comparing the dissociation constants, $K_{d,Cai}$ and $K_{d,Casr}$ (Table 2), which describe the affinity of Ca^{2+} for Ca^{2+}-binding sites to constants reported for Ca^{2+} sensitivity (K_m, $K_{1/2}$). These latter constants reflect the apparent binding of Ca^{2+} to the pump and depend on the experimental conditions as illustrated in Fig. 4, which depicts the pH-dependence of the Ca^{2+} sensitivity curve. To make a direct comparison with values reported in the literature, we calculate the half-maximal binding concentration for $[Ca^{2+}]_i$ from the model under given conditions. For pH values close to 7, half-maximal binding of Ca^{2+} from the cytosol has been measured or calculated to be between 0.5 and 10 μM (21,27,30,31,45). A comparable value is obtained from the model by isolating states P2–P5 (Fig. 2) and plotting the probability of occupying states P4 and P5 as a function of $[Ca^{2+}]_i$. At a pH of 7, the half-maximal point of this curve gives a Ca^{2+} binding constant of 4.88 μM, which is within the range of what is measured in experiments. A similar procedure gives a Ca^{2+} binding constant of 3.6 mM for binding of Ca^{2+} on the luminal side (by calculating the probability of occupying state P6 as a function of $[Ca^{2+}]_{sr}$). This is also consistent with values from the literature of 1.7 mM (46) and 1.48 mM (30). The greater binding affinity of cytosolic Ca^{2+} over luminal Ca^{2+} of approximately three orders of magnitude is a key characteristic of the pump that facilitates the binding of Ca^{2+} from the cytosol (at low concentrations) and the subsequent release of this Ca^{2+} into the luminal environment where $[Ca^{2+}]$ is much higher.

Variable stoichiometry of Ca^{2+} transport

The SERCA model is assumed to have a fixed stoichiometric coupling ratio of 2 Ca^{2+} for every ATP that is hydrolyzed.

Yu and Inesi (47) found that in leak-proof native SR vesicles, the stoichiometry starts to drop below 2 in the absence of oxalate (a chelator of luminal Ca^{2+}) and attribute this drop to a highly elevated luminal Ca^{2+} concentration. Their experiments indicate that this begins to occur ~2 s after the addition of ATP at 25°C. In a rabbit ventricular myocyte, the Ca^{2+} transient lasts for no longer than 500 ms (8) as the SERCA pump is rapidly activated by the increasing cytosolic Ca^{2+} and inactivated when it falls. Therefore, under physiological conditions in the beating heart, it is reasonable to assume that the luminal Ca^{2+} levels do not approach such high levels and therefore the transport of Ca^{2+} is tightly coupled to the hydrolysis of ATP at a stoichiometric ratio of 2.

H^+ binding

The transfer of Ca^{2+} into the SR lumen by the SERCA pump is also accompanied by a counter-transport of H^+ out into the cytosol. At neutral pH, the stoichiometry of the counter-transport between Ca^{2+} and H^+ is measured to be 2:2 (24–26). This is consistent with the prediction of our model of 2 H^+ being counter-transported for 2 Ca^{2+} during each cycle of the pump.

In the enzyme cycle presented in Fig. 1 it was assumed that the H^+ involved in counter-transport had distinct binding sites on the SERCA enzyme. These binding sites were separate from those of the competitive H^+, which competed with Ca^{2+} for the Ca^{2+}-binding sites in the cytosol-facing orientation. However, in the case of the cooperative Ca^{2+} binding model presented in Fig. 2, instead of binding to distinct H^+-binding sites, the binding of the transported H^+ can be interpreted as binding to the Ca^{2+}-binding sites in a scheme that is a slight modification of the one proposed by Yu et al. (25). In this modified scheme, it is proposed that after the two Ca^{2+} have dissociated into the SR lumen, two H^+ then occupy one of the two empty Ca^{2+} binding sites. After SERCA has undergone the conformational change so that the Ca^{2+}-binding sites are now facing the cytosol, the Ca^{2+} binding site that remains empty can subsequently bind a cytosolic Ca^{2+} or H^+. If Ca^{2+} binds, the second Ca^{2+} will rapidly follow and eject the two H^+ occupying the binding site. Yu et al. (26) propose that the binding of H^+ to the Ca^{2+}-binding sites is possible because some of the residues involved in the binding of Ca^{2+} are acidic and are hence capable of exchanging H^+ with Ca^{2+}. Their findings suggest that, assuming the same acidic residues are involved in both H^+ and Ca^{2+} binding, there is a lower affinity for H^+ when the Ca^{2+}-binding sites are in the cytosol-facing orientation, and a higher affinity for H^+ in the luminal orientation. This is indeed the case in the SERCA model presented here where $K_{d,Hi}$ and $K_{d,Hsr}$ for H^+ binding to the cytosol and luminal Ca^{2+}-binding sites are 3.54×10^{-3} and 1.05×10^{-8} mM^{-2}, respectively.

Binding order of partial reactions

The order and placement of the partial reactions involving MgATP binding was shown to be an important determinant of the ability to fit the data set, where an acceptable fit was achieved only when the MgATP binding step was placed before the first Ca^{2+} binding step and after the release of Pi as shown in Fig. 1. For MgATP binding either after the binding of the second Ca^{2+} or after the dissociation of H^+, the model was found to be incompatible with the data.

Reversal of the pump

The SERCA pump has been shown experimentally to be reversible under conditions where the concentrations of MgADP and Pi are high and MgATP is kept very low (48). Under these conditions, the net free energy is positive ($\Delta G_{MgATP} + \Delta G_{SERCA} > 0$), resulting in the efflux of Ca^{2+} from the SR lumen and the synthesis of ATP as the SERCA enzyme cycles in the reverse direction. The thermodynamic constraint imposed on the model (see Methods) ensures that the pump will reverse when the net free energy is zero but the actual rate of cycling in the reverse direction is highly dependent on the kinetics of the model, particularly to the kinetics of MgATP binding (Figs. 9 and 13). At physiological concentrations of MgATP, the model predicts that the reverse rate will be negligible when $\Delta G_{net} > 0$, either by increasing the products of ATP hydrolysis (Fig. 9) or by altering the Ca^{2+} concentrations (Fig. 13) within the physiological range. When the MgATP concentration is kept very low, however,

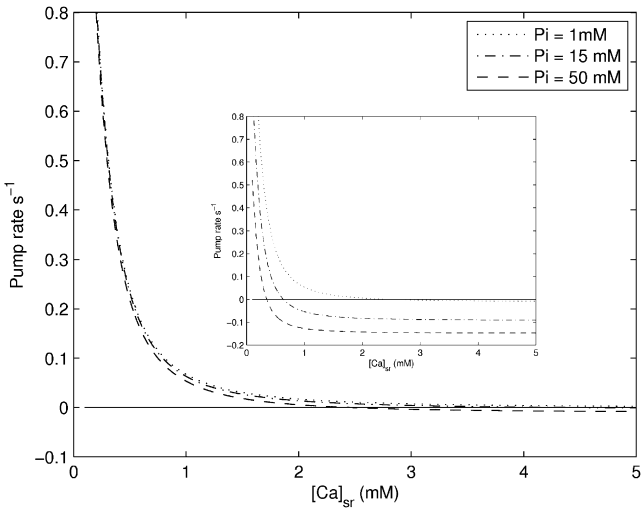

FIGURE 13 An increase in the free $[Ca^{2+}]_{sr}$ leads to a decrease in the pump rate until a reversal point is reached where the pump begins to cycle in the reverse direction. The model predicts that at [MgATP] = 5 mM, the rate at which the pump cycles in reverse is almost negligible over either the physiological or the ischemic range of [Pi]. The inset shows the same set of curves but at the lower [MgATP] of 100 μM. A decrease in [MgATP] reduces the inhibitive effect of MgATP binding resulting in larger reversal rates. Other conditions in the simulation: ADP = 36.3 μM, pH = 7, $[Ca^{2+}]_i$ = 150 nM.

the magnitude of the reversal rates become appreciable as the rate-limiting effect of MgATP binding is reduced. This is consistent with the results of Makinose and Hasselbach (48), where the SERCA pump was shown to reverse when the concentration of MgATP was low.

Data selection

The parameters of the cardiac SERCA model were constrained to a set of data which characterizes the dependence of the pump on the metabolites MgATP, MgADP, and Pi and the ions Ca^{2+} and H^+ (28,41,42). We have sought to use data from cardiac preparations of a single mammalian species and to use data that measured the turnover rate of the pump. While not always possible, we have, within the constraints of available data, sought to maintain species consistency of the model. Considering now the origin of the data, the pH curve and pH-dependent Ca^{2+} curves (28) were from mouse cardiac preparations and therefore intrinsic in those (and hence in the model) is the effect of phospholamban. The ATP/ADP (42) and Pi (41) data, however, are from solubilized SR fragments and nonnative cell expressions of SERCA enzymes of rabbit skeletal muscle, respectively. The justification for using these SERCA enzyme data (from a nonnative source) is that when expressed in the presence of phospholamban, the SERCA1a isoform from skeletal muscle is functionally equivalent to the SERCA2a form in cardiac muscle (28). Because these data represent changing MgATP, MgADP, and Pi concentrations only, and not changing Ca^{2+} concentrations, the presence or absence of phospholamban is not relevant here. In terms of the species difference between mouse and rabbit, there is evidence to suggest their cardiac SERCA pumps have similar characteristics. Under similar pH conditions, the K_m measured in mouse cardiac preparations by Ji et al. (28) of 0.25 μM is very similar to that measured from rabbit ventricular myocytes of 0.26 μM (10). There is also a difference in V_{max} between species, which is due to different expression levels of the SERCA enzyme. The density of cardiac SERCA pumps in mouse is estimated to be higher than that of rabbit (8). In the modeling process, this difference in V_{max} between different data sets is accounted for by normalizing all the data to a single reference point (see Methods). This normalization process also allows for the accounting of temperature differences between data sets when reliable data on Q_{10} values for the various reaction steps are not available. The maximum flux for the pump value was scaled to a value comparable to experiments carried out on rabbit cardiomyocytes at 22°C (see Methods).

Parameter sensitivity

A sensitivity analysis of the model parameters was performed to assess the effects of each parameter on the four data sets. Each of the parameter values in Table 2 was altered by $\pm 10\%$ and the deviation of the resulting curves from the optimal curves (Figs. 4–7) was calculated. The results are presented in Table 3. The sensitivity analysis shows that each of the parameters affects the model fit to at least one set of data and the ability of the model to fit each of the data sets is sensitive to more than one parameter. This is indicative of a model which is not overparameterized in respect of the data used to fit the model parameters, and reflects the whole-pump approach we have taken to fit all four sets of data simultaneously. The parameter with the greatest influence in the model is n, the number of H^+ that are counter-transported for each Ca^{2+}. This parameter has significant effects on the model fit to pH, pH-Ca^{2+}, and ATP curves. The highly sensitive nature of this parameter reflects its importance in determining a well-constrained fit of the model to the data. Taking together the high sensitivity of this parameter and the prediction of $n = 2$ (which is consistent with the literature). This provides us with a good degree of confidence in the optimized model parameters.

The cardiac SERCA model presented here is the first model that incorporates metabolic-sensitivity, Ca^{2+}- and

TABLE 3 The sensitivity of the parameters in the three-state model is quantified by calculating the percentage deviation from the optimal curves given a $\pm 10\%$ change in the parameter value

	pH-Ca^{2+} curve (Fig. 4)			pH curve (Fig. 5)			Pi curve (Fig. 6)			ATP/ADP curve (Fig. 7)		
Parameter	+10%	−10%	Avg.	+10%	−10%	Avg.	+10%	−10%	Avg.	+10%	−10%	Avg.
k_1^+	0	0	0	0	0	0	0	0	0	3.64%	8.51%	6.08%
k_2^+	3.88%	0.70%	2.29%	3.91%	2.89%	3.4%	0	0	0	11.5%	7.52%	9.51%
k_3^+	0.40%	4.52%	2.46%	32.7%	14.1%	23.4%	19.1%	9.40%	13.4%	0.38%	0.37%	0.38%
k_2^-	0	0	0	0	0	0	0	0	0	7.08%	12.9%	10.0%
k_3^-	0	0	0	0	0	0	7.14%	22.2%	23.34%	7.10%	3.50%	5.30%
$k_{d,Cai}$	5.09%	13.6%	9.35%	3.98%	9.97%	6.98%	0	0	0	0	0	0
$k_{d,Casr}$	0	0	0	0	0	0	0	0	0	8.67%	6.22%	7.45%
$k_{d,H1}$	3.58%	0.53%	2.06%	3.70%	2.79%	3.25%	0	0	0	0	0	0
$k_{d,Hi}$	3.88%	0.71%	2.23%	3.89%	2.88%	3.39%	0	0	0	0	0	0
$k_{d,Hsr}$	0.46%	0.18%	0.32%	3.15%	13.74%	8.45%	0.07%	0.07%	0.07%	2.21%	2.87%	2.54%
$k_{d,H}$	0.08%	3.57%	1.83%	22.51%	6.99%	14.8%	17.1%	7.86%	12.5%	1.28%	1.26%	1.27%
n	338%	293%	316%	446%	967%	707%	0.80%	0.58%	0.69%	12.2%	135%	73.6%

The model is most sensitive to n, the number of H^+ that are counter-transported during each pump cycle.

H^+-sensitivity, and thermodynamic constraints into a consistent biophysical framework. Along with the energy-sensitive model of the Na^+/K^+ ATPase (44,49), this model provides a further step toward developing a whole-cell model of cardio-myocyte electrophysiology and Ca^{2+} dynamics that is capable of simulating the effects of compromised metabolism such as ischemia and hypoxia.

APPENDIX

Equations for the three-state cooperative SERCA model

The apparent forward rate constants are

$$\alpha_1^+ = k_1^+[\mathrm{MgATP}],$$

$$\alpha_2^+ = \frac{k_2^+\tilde{\mathrm{Ca}}_i^2}{\tilde{\mathrm{Ca}}_i^2(1+\tilde{\mathrm{H}}_i)+\tilde{\mathrm{H}}_i(1+\tilde{\mathrm{H}}_1)},$$

$$\alpha_3^+ = \frac{k_3^+\tilde{\mathrm{H}}_{sr}}{\tilde{\mathrm{H}}\left(1+\tilde{\mathrm{Ca}}_{sr}^2\right)+\tilde{\mathrm{H}}_{sr}(1+\tilde{\mathrm{H}})}, \quad (10)$$

and the apparent backward rate constants are

$$\alpha_1^- = \frac{k_1^-\tilde{\mathrm{H}}_i}{\tilde{\mathrm{Ca}}_i^2(1+\tilde{\mathrm{H}}_i)+\tilde{\mathrm{H}}_i(1+\tilde{\mathrm{H}}_1)},$$

$$\alpha_2^- = \frac{k_2^-[\mathrm{MgADP}]\tilde{\mathrm{Ca}}_{sr}^2\tilde{\mathrm{H}}_{sr}}{\tilde{\mathrm{H}}\left(1+\tilde{\mathrm{Ca}}_{sr}^2\right)+\tilde{\mathrm{H}}_{sr}(1+\tilde{\mathrm{H}})},$$

$$\alpha_3^- = k_3^-[\mathrm{Pi}], \quad (11)$$

where

$$\tilde{\mathrm{Ca}}_i = \frac{[\mathrm{Ca}^{2+}]_i}{K_{d,Cai}},\ \tilde{\mathrm{H}}_i = \frac{[\mathrm{H}^+]}{K_{d,Hi}},\ \tilde{\mathrm{H}}_1 = \frac{[\mathrm{H}^+]}{K_{d,H1}},$$

$$\tilde{\mathrm{Ca}}_{sr} = \frac{[\mathrm{Ca}^{2+}]_{sr}}{K_{d,Casr}},\ \tilde{\mathrm{H}}_{sr} = \frac{[\mathrm{H}^+]}{K_{d,Hsr}},\ \tilde{\mathrm{H}} = \frac{[\mathrm{H}^+]}{K_{d,H}}, \quad (12)$$

$$k_1^- = \frac{k_1^+k_2^+k_3^+K_{d,Casr}^2K_{d,Hi}K_{d,H}}{k_2^-k_3^-K_{d,Cai}^2K_{d,Hsr}e^{\Delta G^o_{MgATP}/RT}}, \quad (13)$$

$\Delta G^o_{MgATP} = 11.9\ \mathrm{kJ\ mol^{-1}}$, $R = 8.314\ \mathrm{JK^{-1}\ mol^{-1}}$, and T is the temperature in K. The cycling rate (in units of s^{-1}) is given by

$$\nu_{cycle} = \frac{\alpha_1^+\alpha_2^+\alpha_3^+ - \alpha_1^-\alpha_2^-\alpha_3^-}{\Sigma_3}, \quad (14)$$

where Σ_3 is a sum of nine products given by

$$\Sigma_3 = \alpha_2^+\alpha_3^+ + \alpha_1^-\alpha_3^+ + \alpha_1^-\alpha_2^- + \alpha_1^+\alpha_3^+ + \alpha_2^-\alpha_1^+ \ldots + \alpha_2^-\alpha_3^- + \alpha_1^+\alpha_2^+ + \alpha_3^-\alpha_1^- + \alpha_3^-\alpha_2^+. \quad (15)$$

Equations for the two-state SERCA model

The apparent forward rate constants are

$$\alpha_1^+ = \frac{k_2^+\tilde{\mathrm{MgATP}}\tilde{\mathrm{Ca}}_i^2}{\tilde{\mathrm{MgATP}}\tilde{\mathrm{Ca}}_i^2 + \tilde{\mathrm{H}}_i\left(1+\tilde{\mathrm{MgATP}}\left(1+\tilde{\mathrm{H}}_1+\tilde{\mathrm{Ca}}_i^2\right)\right)},$$

$$\alpha_2^+ = \frac{k_3^+\tilde{\mathrm{H}}_{sr}}{\tilde{\mathrm{H}}_{sr}(1+\tilde{\mathrm{H}})+\tilde{\mathrm{H}}\left(1+\tilde{\mathrm{Ca}}_{sr}^2\right)}, \quad (16)$$

and the apparent backward rate constants are

$$\alpha_1^- = \frac{k_2^-[\mathrm{MgADP}]\tilde{\mathrm{Ca}}_{sr}^2\tilde{\mathrm{H}}}{\tilde{\mathrm{H}}_{sr}(1+\tilde{\mathrm{H}})+\tilde{\mathrm{H}}\left(1+\tilde{\mathrm{Ca}}_{sr}^2\right)},$$

$$\alpha_2^- = \frac{k_3^-[\mathrm{Pi}]\tilde{\mathrm{H}}_i}{\tilde{\mathrm{MgATP}}\tilde{\mathrm{Ca}}_i^2 + \tilde{\mathrm{H}}_i\left(1+\tilde{\mathrm{MgATP}}\left(1+\tilde{\mathrm{H}}_1+\tilde{\mathrm{Ca}}_i^2\right)\right)}, \quad (17)$$

where

$$\tilde{\mathrm{MgATP}} = \frac{[\mathrm{MgATP}]}{K_{d,ATP}}, \quad (18)$$

$$K_{d,ATP} = \frac{k_1^-}{k_1^+} = \frac{k_2^+k_3^+K_{d,Casr}^2K_{d,Hi}K_{d,H}}{k_2^-k_3^-K_{d,Cai}^2K_{d,Hsr}e^{\Delta G^o_{MgATP}/RT}}, \quad (19)$$

$\Delta G^o_{MgATP} = 11.9\ \mathrm{kJ\ mol^{-1}}$, $R = 8.314\ \mathrm{JK^{-1}\ mol^{-1}}$, and T is the temperature in K. The cycling rate (in units of s^{-1}) is given by

$$\nu_{cycle} = \frac{\alpha_1^+\alpha_2^+ - \alpha_1^-\alpha_2^-}{\Sigma_2}, \quad (20)$$

where Σ_2 is a sum of four terms given by

$$\Sigma_2 = \alpha_1^+ + \alpha_2^+ + \alpha_1^- + \alpha_2^-. \quad (21)$$

Model code

The model is available in the CellML database (50,51). The MatLab code for reproducing the plots in the article is available from the author.

The authors acknowledge valuable comments from Jonna Terkildsen.

This work was supported by a Tertiary Education Commission (New Zealand) Top Achiever Doctoral Scholarship and a Royal Society of New Zealand travel grant to K.T.; Royal Society of New Zealand (Marsden Fund No. 06-UoA-123) to D.S.L. and N.P.S.; National Institute of Biomedical Imaging and Bioengineering grant No. EB-005825 to E.J.C. and N.P.S.; and an Engineering and Physical Sciences Research Council grant No. EP/G007521/1 to N.P.S.

REFERENCES

1. Crampin, E. J., M. Halstead, P. Hunter, P. Nielsen, D. Noble, et al. 2004. Computational physiology and the physiome project. *Exp. Physiol.* 89:1–26.

2. Noble, D., A. Varghese, P. Kohl, and P. Noble. 1998. Improved guinea-pig ventricular cell model incorporating a diadic space, I-Kr and I-Ks, and length- and tension-dependent processes. *Can. J. Cardiol.* 14:123–134.
3. Winslow, R. L., J. Rice, S. Jafri, E. Marban, and B. O'Rourke. 1999. Mechanisms of altered excitation-contraction coupling in canine tachycardia-induced heart failure, II: model studies. *Circ. Res.* 84:571–586.
4. Faber, G. M., and Y. Rudy. 2000. Action potential and contractility changes in $[N^+]_i$ overloaded cardiac myocytes: a simulation study. *Biophys. J.* 78:2392–2404.
5. Matsuoka, S., N. Sarai, S. Kuratomi, K. Ono, and A. Noma. 2003. Role of individual ionic current systems in ventricular cells hypothesized by a model study. *Jpn. J. Physiol.* 53:105–123.
6. ten Tusscher, K. H. W. J., and A. V. Panfilov. 2006. Alternans and spiral breakup in a human ventricular tissue model. *Am. J. Physiol. Heart Circ. Physiol.* 291:H1088–H1100.
7. Smith, N. P., and E. J. Crampin. 2004. Development of models of active ion transport for whole-cell modeling: cardiac sodium-potassium pump as a case study. *Prog. Biophys. Mol. Biol.* 85:387–405.
8. Bers, D. M. 2001. Excitation-Contraction Coupling and Cardiac Contractile Force, 2nd Ed. Kluwer Academic Publishers, Dordrecht, The Netherlands.
9. Tanford, C. 1982. Steady-state of an ATP-driven calcium-pump—limitations on kinetic and thermodynamic parameters. *Proc. Natl. Acad. Sci. USA.* 79:6161–6165.
10. Shannon, T. R., K. S. Ginsburg, and D. M. Bers. 2000. Reverse mode of the sarcoplasmic reticulum calcium pump and load-dependent cytosolic calcium decline in voltage-clamped cardiac ventricular myocytes. *Biophys. J.* 78:322–333.
11. Gould, G. W., J. M. East, R. J. Froud, J. M. McWhirter, H. I. Stefanova, et al. 1986. A kinetic model for the $Ca^{2+} + Mg^{2+}$-activated ATPase of sarcoplasmic reticulum. *Biochem. J.* 237:217–227.
12. Haynes, D. H., and A. Mandveno. 1987. Computer modeling of Ca^{2+} pump function of Ca^{2+}-Mg^{2+}-ATPase of sarcoplasmic-reticulum. *Physiol. Rev.* 67:244–284.
13. Makinose, M. 1973. Possible functional-states of enzyme of sarcoplasmic calcium-pump. *FEBS Lett.* 37:140–143.
14. de Meis, L., and A. L. Vianna. 1979. Energy interconversion by the Ca^{2+}-dependent ATPase of the sarcoplasmic reticulum. *Annu. Rev. Biochem.* 48:275–292.
15. Dupont, Y. 1982. Low-temperature studies of the sarcoplasmic-reticulum calcium-pump mechanism of calcium-binding. *Biochim. Biophys. Acta.* 688:75–87.
16. Petithory, J. R., and W. P. Jencks. 1988. Sequential dissociation of Ca^{2+} from the calcium adenosine-triphosphatase of sarcoplasmic-reticulum and the calcium requirement for its phosphorylation by ATP. *Biochemistry.* 27:5553–5564.
17. Inesi, G. 1987. Sequential mechanism of calcium-binding and translocation in sarcoplasmic-reticulum adenosine-triphosphatase. *J. Biol. Chem.* 262:16338–16342.
18. Orlowski, S., and P. Champeil. 1991. Kinetics of calcium dissociation from its high-affinity transport sites on sarcoplasmic-reticulum ATPase. *Biochemistry.* 30:352–361.
19. Forge, V., E. Mintz, D. Canet, and F. Guillain. 1995. Lumenal Ca^{2+} dissociation from the phosphorylated Ca^{2+}-ATPase of the sarcoplasmic-reticulum is sequential. *J. Biol. Chem.* 270:18271–18276.
20. Mintz, E., and F. Guillain. 1997. Ca^{2+} transport by the sarcoplasmic reticulum ATPase. *Biochim. Biophys. Acta Bioenerg.* 1318:52–70.
21. Inesi, G., M. Kurzmack, C. Coan, and D. E. Lewis. 1980. Cooperative calcium-binding and ATPase activation in sarcoplasmic-reticulum vesicles. *J. Biol. Chem.* 255:3025–3031.
22. Madeira, V. M. C. 1978. Proton gradient formation during transport of Ca^{2+} by sarcoplasmic-reticulum. *Arch. Biochem. Biophys.* 185:316–325.
23. Chiesi, M., and G. Inesi. 1980. Adenosine 5′-triphosphate dependent fluxes of manganese and hydrogen-ions in sarcoplasmic-reticulum vesicles. *Biochemistry.* 19:2912–2918.
24. Levy, D., M. Seigneuret, A. Bluzat, and J. L. Rigaud. 1990. Evidence for proton countertransport by the sarcoplasmic-reticulum Ca^{2+}-ATPase during calcium-transport in reconstituted proteoliposomes with low ionic permeability. *J. Biol. Chem.* 265:19524–19534.
25. Yu, X., S. Carroll, J. L. Rigaud, and G. Inesi. 1993. H^+ countertransport and electrogenicity of the sarcoplasmic-reticulum Ca^{2+} pump in reconstituted proteoliposomes. *Biophys. J.* 64:1232–1242.
26. Yu, X., L. N. Hao, and G. Inesi. 1994. A pK change of acidic residues contributes to cation countertransport in the Ca-ATPase of sarcoplasmic-reticulum—role of H^+ in Ca^{2+}-ATPase countertransport. *J. Biol. Chem.* 269:16656–16661.
27. Inesi, G., L. Chen, C. Sumbilla, D. Lewis, and M. E. Kirtley. 1995. Ca^{2+} binding and translocation by the sarcoplasmic reticulum ATPase: Functional and structural considerations. *Biosci. Rep.* 15:327–339.
28. Ji, Y., E. Loukianov, T. Loukianova, L. R. Jones, and M. Periasamy. 1999. SERCA1a can functionally substitute for SERCA2a in the heart. *Am. J. Physiol. Heart Circ. Physiol.* 276:H89–H97.
29. Vianna, A. L. 1975. Interaction of calcium and magnesium in activating and inhibiting nucleoside triphosphatase of sarcoplasmic-reticulum vesicles. *Biochim. Biophys. Acta.* 410:389–406.
30. Pickart, C. M., and W. P. Jencks. 1984. Energetics of the calcium-transporting ATPase. *J. Biol. Chem.* 259:1629–1643.
31. Cantilina, T., Y. Sagara, G. Inesi, and L. R. Jones. 1993. Comparative-studies of cardiac and skeletal sarcoplasmic-reticulum ATPases—effect of a phospholamban antibody on enzyme activation by Ca^{2+}. *Circulation.* 88:624–629.
32. Hill, T. L. 1989. Free Energy Transduction and Biochemical Cycle Kinetics. Springer-Verlag, New York.
33. Tanford, C., J. A. Reynolds, and E. A. Johnson. 1987. Sarcoplasmic-reticulum calcium-pump—a model for Ca^{2+} binding and Ca^{2+}-coupled phosphorylation. *Proc. Natl. Acad. Sci. USA.* 84:7094–7098.
34. MacLennan, D. H., C. J. Brandl, B. Korczak, and N. M. Green. 1985. Amino-acid sequence of a $Ca^{2+} + Mg^{2+}$-dependent ATPase from rabbit muscle sarcoplasmic-reticulum, deduced from its complementary DNA sequence. *Nature.* 316:696–700.
35. Brandl, C. J., N. M. Green, B. Korczak, and D. H. MacLennan. 1986. 2 Ca^{2+} ATPase genes—homologies and mechanistic implications of deduced amino-acid sequences. *Cell.* 44:597–607.
36. Peinelt, C., and H. J. Apell. 2005. Kinetics of Ca^{2+} binding to the SR Ca-ATPase in the E-1 state. *Biophys. J.* 89:2427–2433.
37. Bassani, J. W. M., R. A. Bassani, and D. M. Bers. 1994. Relaxation in rabbit and rat cardiac-cells—species-dependent differences in cellular mechanisms. *J. Physiol.* 476:279–293.
38. Levitsky, D. O., D. S. Benevolensky, T. S. Levchenko, V. N. Smirnov, and E. I. Chazov. 1981. Calcium-binding rate and capacity of cardiac sarcoplasmic-reticulum. *J. Mol. Cell. Cardiol.* 13:785–796.
39. Shigekawa, M., J. M. Finegan, and A. M. Katz. 1976. Calcium-transport ATPase of canine cardiac sarcoplasmic-reticulum—comparison with that of rabbit fast skeletal-muscle sarcoplasmic-reticulum. *J. Biol. Chem.* 251:6894–6900.
40. Kennedy, J., and R. Eberhart. 1995. Particle swarm optimization. 1995 IEEE International Conference On Neural Networks Proceedings, Vols. 1–6:1942–1948.
41. Dode, L., B. Vilsen, K. V. Baelen, F. Wuytack, J. D. Clausen, et al. 2002. Dissection of the functional differences between sarco(endo)plasmic reticulum Ca^{2+}-ATPase (SERCA) 1 and 3 isoforms by steady-state and transient kinetic analyses. *J. Biol. Chem.* 277:45579–45591.
42. Sakamoto, J., and Y. Tonomura. 1980. Order of release of ADP and Pi from phosphoenzyme with bound ADP of Ca^{2+}-dependent ATPase from sarcoplasmic reticulum and of Na^+, K^+-dependent ATPase studied by ADP-inhibition patterns. *J. Biochem. (Tokyo).* 87:1721–1727.
43. Befroy, D. E., T. Powell, G. K. Radda, and K. Clarke. 1999. Osmotic shock: modulation of contractile function, pH_i, and ischemic damage in perfused guinea pig heart. *Am. J. Physiol. Heart Circ. Physiol.* 276:H1236–H1244.

44. Terkildsen, J. R., E. J. Crampin, and N. P. Smith. 2007. The balance between inactivation and activation of the Na^+-K^+ pump underlies the triphasic accumulation of extracellular K^+ during myocardial ischemia. *Am. J. Physiol. Heart Circ. Physiol.* 293:H3036–H3045.

45. Meissner, G. 1973. ATP and Ca^{2+} binding by Ca^{2+} pump protein of sarcoplasmic reticulum. *Biochim. Biophys. Acta.* 298:906–926.

46. Inesi, G., C. Sumbilla, and M. E. Kirtley. 1990. Relationships of molecular-structure and function in Ca^{2+}-transport ATPase. *Physiol. Rev.* 70:749–760.

47. Yu, X., and G. Inesi. 1995. Variable stoichiometric efficiency of Ca^{2+} and Sr^{2+} transport by the sarcoplasmic-reticulum ATPase. *J. Biol. Chem.* 270:4361–4367.

48. Makinose, M., and W. Hasselbach. 1971. ATP synthesis by reverse of sarcoplasmic calcium pump. *FEBS Letters.* 12:271–272.

49. Crampin, E. J., and N. P. Smith. 2006. A dynamic model of excitation-contraction coupling during acidosis in cardiac ventricular myocytes. *Biophys. J.* 90:3074–3090.

50. Lloyd, C., J. Lawson, P. Hunter, and P. Nielsen. 2008. The CellML Model Repository. *Bioinformatics.* 24:2122–2123.

51. Terkildsen, J. R., S. Niederer, E. J. Crampin, P. Hunter, and N. P. Smith. 2008. Using physiome standards to couple cellular functions for rat cardiac excitation-contraction. *Exp. Physiol.* 93:919–929.